Delft University of Technology

Concept and design of a metastructure-based multi-stable surface
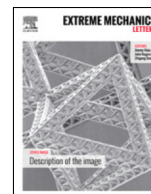
Zhang, Yong; Tichem, Marcel; van Keulen, Fred

Important note
To cite this publication, please use the final published version (if applicable).
Please check the document version above.

Concept and design of a metastructure-based multi-stable surface

Yong Zhang [*], Marcel Tichem, Fred van Keulen

Department of Precision and Microsystems Engineering, Delft University of Technology, Mekelweg 2, 2628 CD, Delft, The Netherlands

ARTICLE INFO

ABSTRACT

Metastructures composed of snapping beams are capable of deforming into a series of stable states, enabling them to realize shape reconfigurations. In this paper, we present the design of a metastructure-based morphing surface that is able to exhibit a series of stable configurations with different curvatures. Using theoretical, numerical, and experimental approaches, we study the snap-through transition between the initially flat and the curved stable configurations. Effects of geometric parameters on the snap-through and curvatures are systematically investigated. Results show that the beam thickness is important for tuning the snap-through response, while the curvature can be tuned by changing the beam height and the horizontal span of the structures. Furthermore, an analytical model is developed to investigate the structural nonlinear deformations. It is shown that the proposed model can predict the snap-through transition properly. The structural stability can be controlled by setting proper values for t/L and h/L (t, h, and L represents the beam thickness, height and span, respectively). Finally, it is demonstrated that based on two-dimensional arrangements of bi-stable elements, various stable configurations, like corrugations in different directions, can be imposed to the surface.

1. Introduction

Imparting a curvature change to a surface is important for applications of morphing airfoils [1–4], deployable structures [5,6], adaptive optical devices [7–9], and fluid control [10,11]. Surfaces that are capable of changing their shapes into a series of deformed configurations are often referred to as morphing surfaces [12,13]. The reconfigurability of morphing surfaces makes it possible to realize tunable functionalities. For instance, a change of surface topography can lead to different focal properties for optical display applications [14]. To retain a curved surface, bi-stability has been commonly explored to avoid prolonged actuation after shape reconfiguration.

In order to realize stable configurations, various bi-stable structural prototypes, e.g., compliant plates and shells, have been presented in literature [15,16]. For instance, one type of bi-stable morphing structures is the composite laminate shell, which can exhibit two stable cylindrical shapes [17]. The bi-stability is mainly attributed to residual stresses introduced during the manufacturing process, causing the shell to be curved after cooling. Thus, the laminated shells' mechanical properties and stable configurations are highly dependent on the laminate's in-plane layups [18]. However, there are a few limitations for the bi-stable laminated shells, namely, (i) they are difficult to fabricate at small scale; (ii) the choice of materials is limited. Alternatively, bi-stable

behavior can be achieved by using homogeneous materials in a spherical cap-type shell design [19–21]. Under compression, the cap-shaped shells can flip into an 'inverted' stable state. Analytical and numerical studies have demonstrated that the snap-through transition of the spherical shells can be tuned by changing the shell's geometry, such as thickness and radius [22,23]. Moreover, Loukaides et al. [24] extended these cap-shaped shells to a grid-shell design with inner structures, for which the snap-through transition can be further manipulated by tuning local geometries.

Apart from bi-stability, multi-stable behavior can also be implemented into morphing surfaces. From the perspective of structural morphing, multi-stability allows for more versatile designs. To achieve this, a few studies have focused on connecting multiple bi-stable shells to design multi-stable structures. Following this strategy, many multi-stable surfaces have been presented [25–30]. For example, Dai et al. [26] designed a type of morphing surfaces by assembling few bi-stable shells, demonstrating the potential to realize a wavy skin for shape morphing. Cui et al. [25] characterized the coupling effects between bi-stable elements and demonstrated a quad-stable surface design. However, the mechanical response of these multi-stable surfaces can be significantly affected by the joints and only a few stable configurations, e.g., cylindrical shapes, can be achieved.

To enrich the degree of multi-stability, we propose and study a new concept of morphing surface design, for which multi-stable beam-type metastructures (MBMs) are exploited to control deformations of the surface. MBMs are periodic structures that feature bi-stable snapping beams [31–36]. In terms of kinematics,

* Corresponding author.
    E-mail address: Y.Zhang-15@tudelft.nl (Y. Zhang).

(a) Bi-stable element

(b) Morphing surface design

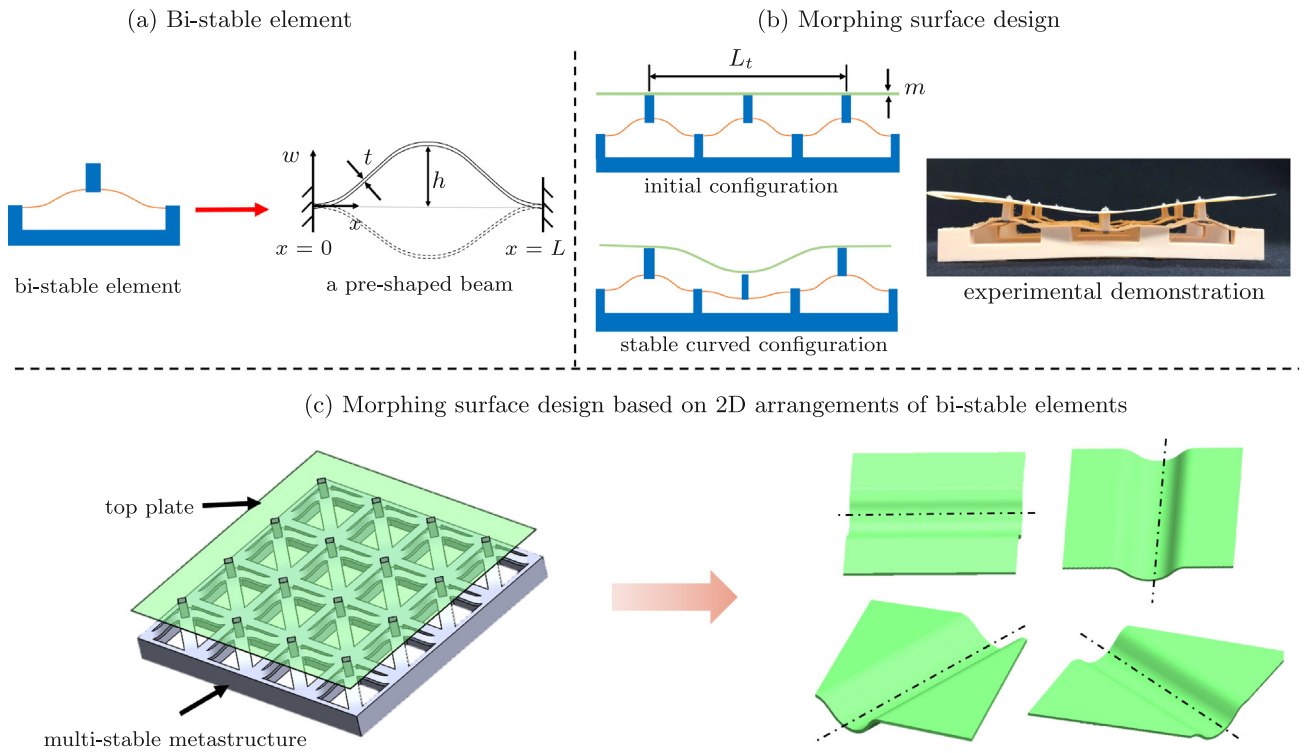(c) Morphing surface design based on 2D arrangements of bi-stable elements

Fig. 1. Schematic diagram of the proposed multi-stable surface design. (a) For each bi-stable element, a pre-shaped curved beam is able to snap into a second stable state (illustrated by curved dashed lines). (b) Morphing surface design. A thin compliant plate is connected with a multi-stable metastructure here composed of three bi-stable elements. When the center element snaps, the plate can stabilize at the curved configuration. Picture on the right shows an experimental demonstration of the stable curved configuration. (c) Morphing surface design based on 2D arrangements of bi-stable elements. When multiple bi-stable elements snap, the curved stable configurations can be oriented in different directions, as depicted by the dot lines.

multi-stable metastructures are capable of realizing a large translational motion via snap-through behavior, creating opportunities for motion-related applications. For instance, Bobbert et al. [37] designed deployable implants based on MBMs. Liu et al. [38] demonstrated the application of MBMs in motion systems. From these demonstrations it can be noted that the MBMs' stable configurations can be programmed by a proper arrangement of the unit cells. Subsequently, these arrangements can serve as the basis for designing morphing surfaces with new features. To the best of our knowledge, the potential of using MBMs to control surface morphology has not been studied, and the associated design requirements are still unclear.

In this work, we investigate the possibility of using MBMs to impart curvature changes to a surface and study the accessible stable configurations. In Section 2, we present the design concept and discuss the stable curved configurations. Effects of geometric parameters on the curved states are studied both experimentally and numerically in Section 3. Moreover, an analytical model is proposed to examine the design criteria for ensuring stability of the structure. In Section 4, we extend the MBM design to a two-dimensional (2D) arrangement of unit cells and investigate the corresponding stable configurations. Conclusions are presented in Section 5.

2. Design concept and methods

2.1. Structural design

The proposed design concept is based on multi-stable metastructures consisting of an array of bi-stable elements. As shown in Fig. 1(a), a pre-shaped curved beam (marked in orange) plays a pivotal role in ensuring bi-stable behavior. When an applied load

exceeds a critical value, the pre-shaped beam can exhibit snap-through behavior and is capable of maintaining the deformed configuration (denoted by the dashed line) after removing the applied loads [39]. The beam's initial shape ($w(x)$) can be expressed as:

$$w(x) = \frac{h}{2}(1 - \cos(\pi\frac{2x}{L})), \tag{1}$$

where x represents a horizontal coordinate, and h, L denote the beam height and length, respectively. In-plane and out-of-plane thickness are denoted as t and b, respectively (see Fig. 1(a)). Next, the morphing surface is realized by connecting a compliant plate with a multi-stable metastructure. As illustrated in Fig. 1(b), the multi-stable metastructure here consists of three bi-stable elements that are arranged in one direction (1D), and a thin plate (marked in green) is connected to the multi-stable metastructure at the top. As depicted in this figure, L_t and m represent the top plate's effective span and thickness, respectively. The plate's curvature can be controlled by deforming a bi-stable element. For example, flipping the center bi-stable element can result in stable local curvature that can be retained without supplying actuation (see Fig. 1(b)). This deformed state with local curvature is referred to as stable curved configuration in the remainder of this paper. Fig. 1(b) also presents an experimental demonstration of the same design.

Next to the 1D arrangement, bi-stable elements can be arranged in two directions to design morphing surfaces. Fig. 1(c) shows a multi-stable metastructure comprising two-dimensional (2D) arrangements of bi-stable elements. By connecting this metastructure with a compliant plate, it is possible to achieve stable curved configurations oriented in multiple directions, which results from a collective effect of the plate's compliance and the
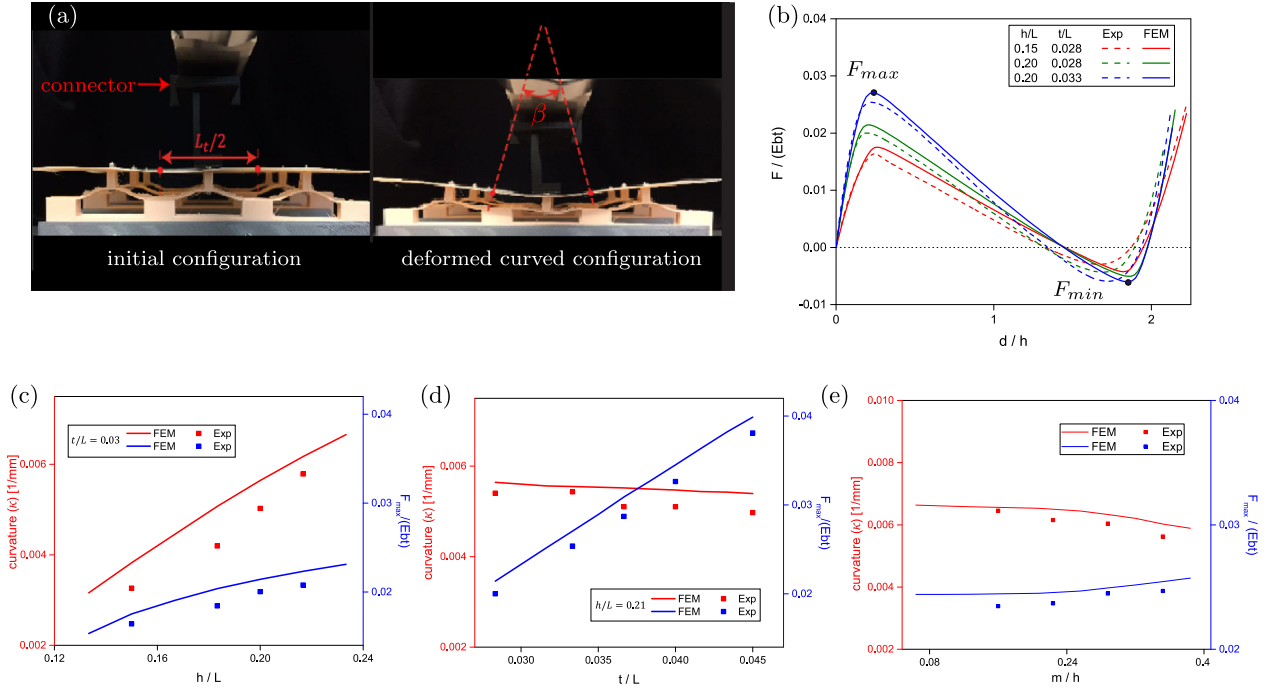
Fig. 2. The snap-through transition from the initial to the curved configuration. (a) The displacement-controlled loading is applied at the center of top plate, resulting in the deformed curved configuration. (b) Measured and simulated force–displacement curves for different samples (L = 30 mm, m = 1.2 mm). (c)–(d) The curvature κ of the stable configuration and the maximum force F_{max} are plotted as a function of h/L and t/L, respectively. (e) Effect of m on the curvature κ and the force F_{max}.

beams' bi-stability. As illustrated by the dot lines in Fig. 1(c), the curved configuration of the surface can be oriented in different directions. Note that it is possible to realize multiple curved configurations simultaneously (see Fig. 7(d)). To explore this further, morphing surfaces based on 2D arrangements of bi-stable elements are designed in Section 4.

2.2. Fabrication and experiments

Samples are fabricated based on a process of 3D printing and manual assembly. Specifically, the multi-stable metastructures are manufactured using a fused deposition printer (Prusa MK3s) with thermoplastic elastomers (TPU, Flex-45). In this work, the thin plates are printed with the same material. Then, the multi-stable metastructure and the thin plate are connected using screws. In order to determine material properties of TPU, standard tensile measurements are performed on multiple printed dumbbell specimens according to the ASTM D638-14 standard (see Supporting Materials, Appendix A), where the measured maximum elastic strain of Flex-45 is in the range of 55%–60%.

Uniaxial loading tests are carried out to investigate the snap-through transition. A universal testing system (Zwick-005) is used to exert displacement-controlled loading. Rigid connectors are printed with stiff material (polylactide) for connecting the machine head with specimens. Detailed information on the rigid connector can be found in Supporting Materials. During the loading, the displacement of the top is controlled with a speed of 10 mm/min, while the bottom of a sample is fully clamped. Moreover, the curvature of the deformed top plate is characterized experimentally. It can be noted that the plate's curvature at the deformed state is not uniform (see Fig. 1(b)). Here, an average curvature (denoted as κ) is defined. As shown in Fig. 2(a), two red markers with a distance of $L_t/2$ are added to the undeformed plate and we take photographs of the deformed curved configurations. Using image analysis software (ImageJ), lines perpendicular to the plate at the two markers are drawn, forming an angle β,

as highlighted in Fig. 2(a). Then, the average curvature κ is given by:

$$\kappa = \frac{2\beta}{L_t}. \tag{2}$$

Note that in this study β is in the range of 10°–20°. In case of large angles, it is suggested to fit the curved profile with polynomial functions for characterizing the curvature.

2.3. Numerical simulations

Finite element models (FEM) based on ABAQUS/Standard (2017) are used to simulate snap-through transitions. The measured stress–strain curves of TPU are imported into the FEM, in which a hyper-elastic material model (Marlow potential [40]) is adopted. Note that the material parameters in FEM are based on the TPU's hyperelastic behavior as the maximum strain of structural deformations is in the order of 15%, which is lower than that of TPU, i.e., 55%. Eight-node solid elements (C3D8) are used and mesh convergence studies have been conducted to ensure accuracy. Boundary conditions are defined in such a way that the bottom of the structures is fully constrained and displacements are applied on the top. The reaction force is collected from the nodes with prescribed displacements. Note that the mean curvature κ is also quantified numerically.

3. Stable curved configuration

As discussed in Section 2.1, the structural snap-through transition involves deformations of both the metastructure and the top plate. In order to reveal the mechanical characteristics, in this section, snap-through transitions from the initial to the deformed curved configurations are investigated. Effects of geometric parameters are analyzed both experimentally and numerically. Moreover, to enable a deep understanding of the mechanical response, an analytical model is developed.
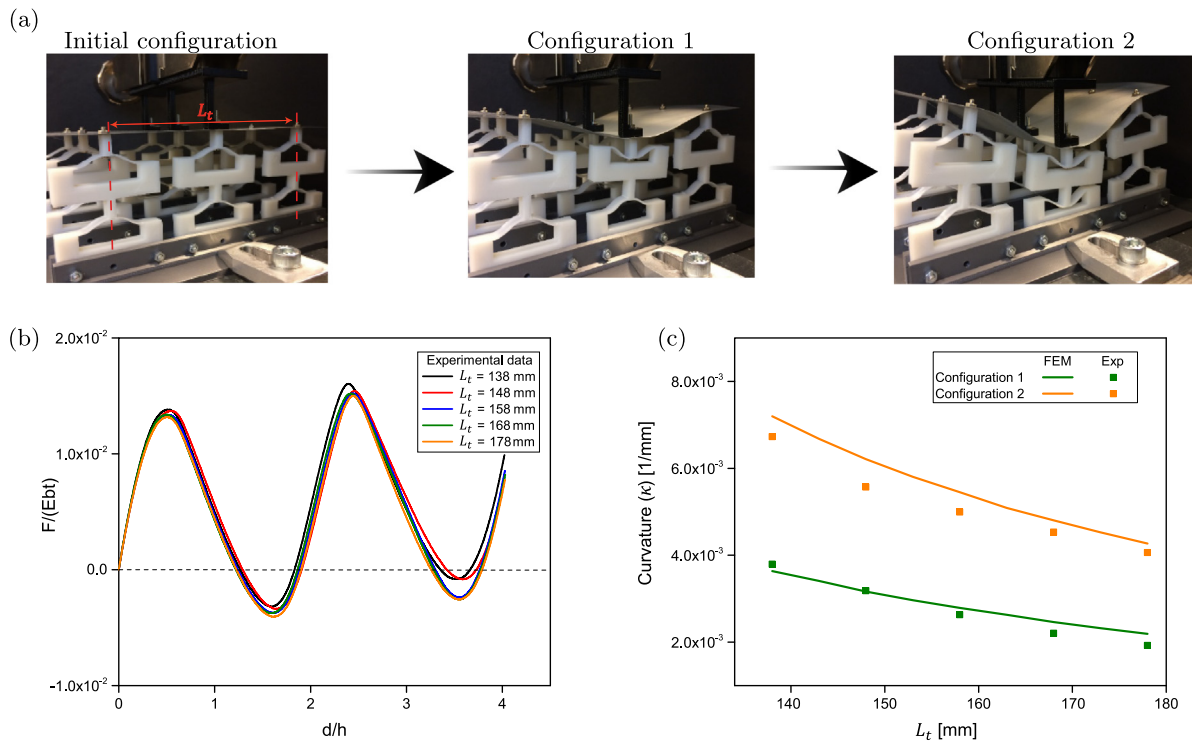
Fig. 3. Curved stable configurations of a compliant plate connected with a two-layer multi-stable metastructure. (a) The two-layer structure is composed of multiple bi-stable elements ($t = 0.85$ mm, $h = 6$ mm, $L = 40$ mm). Snapshots of structural deformations during uniaxial loading are shown. The first and second deformed stable configuration are denoted as Configuration 1 and 2, respectively. (b) Experimentally measured force–displacement responses for different L_t. (c) The measured and simulated κ of Configuration 1 and 2 as a function of L_t.

3.1. Snap-through transitions

As shown in Fig. 2(a), the snap-through transition from the initial flat to the deformed curved configuration is characterized. Fig. 2(b) presents force–displacement curves for multiple structures with different geometric parameters, where the force (F) and displacement (d) are normalized by Ebt and h. E represents Young's modulus of the material. In the figure, it can be noted that the structure first exhibits a positive tangent stiffness before reaching the maximum force (denoted as F_{max}). Next, the structure exhibits a negative tangent stiffness during the continued loading until the minimum force (F_{min}) is reached. Finally, the structure snaps into the stable curved configuration with a positive tangent stiffness. The discrepancy between experimental and numerical results is mainly caused by the manufacturing imperfections, e.g., a slight variation of the thickness and curvature of the structure. Moreover, it can be noted that during loading the center bi-stable elements snap while the adjacent beam elements (left and right beside the center element) are rotated, causing the force–displacement curves to be different from that of a single pre-shaped beam. Specifically, deformations of the adjacent elements and the top surface cause the metastructure to exhibit a larger F_{max} and a smaller absolute value of F_{min} than the single pre-shaped beam (see Supporting Materials, Appendix A). This happens because during the loading, the adjacent elements and the top surface generate resistance against the snap-through of the center element. To characterize the rotations of the adjacent elements, an analytical study has been performed in the following section. Furthermore, experimental and numerical results indicate that the snap-through response is dependent on both h/L and t/L, as a result of the beam's bi-stability. For instance, increasing h/L leads to an evident change of F_{max}, as presented in the figure. The resulting curvature κ is also influenced by t/L and h/L. In order to evaluate the effect of geometric parameters on the snap-through, a parametric study is performed.

Results for metastructures with different geometries are presented in Fig. 2(c)–(d), where κ and F_{max} are plotted as a function of h/L and t/L. In these two figures, it can be seen that κ is more sensitive to h/L than t/L such that increasing h/L leads to a distinct change of κ, while varying t/L has a minor effect on κ. This is because the displacement from the initial to curved configuration is mainly determined by h rather than t. In contrast, it can be noted that t/L is more influential for tuning F_{max} when compared to h/L (see Fig. 2(d)). This is due to the fact that as t increases, the beam's bending and axial stiffness will increase significantly, leading to a stiffer mechanical response. In case of varying h, the change of structural bending stiffness is not as large as that for t, resulting in a smaller change of F_{max}. In addition, the snap-through behavior can also be influenced by the top plate. Here, effect of the plate thickness m is studied, and Fig. 2(e) plots the variation of κ and F_{max} for different thickness. As presented in the figure, with the increase of m, F_{max} gradually increases due to the enlarged bending stiffness of the plate. Note that in this paper, the thin plate has a small thickness to span ratio such that the influence of m on F_{max} is not as evident as that of h and t, demonstrating that the bi-stable elements play a major role in the structural deformations. Moreover, it can be seen that the average curvature κ exhibits a small decrease when m increases.

Next, we study the curved configurations for a compliant plate connected with a two-layer multi-stable metastructure. Multiple bi-stable elements are arranged in horizontal and vertical directions, as shown in Fig. 3(a). During uniaxial loading, the structure is able to stabilize at each of two deformed configurations (denoted as Configuration 1 and 2), indicating if only one of the serial bi-stable elements is flipped, or both. Note that here the center element at the top layer first snap, as shown in Configuration 1. It is possible that the element at the bottom layer snap first. The snapping sequence (i.e., which layer first snaps) is mainly determined by inevitable manufacturing imperfections. That is, the layer with lower critical load will snap first.
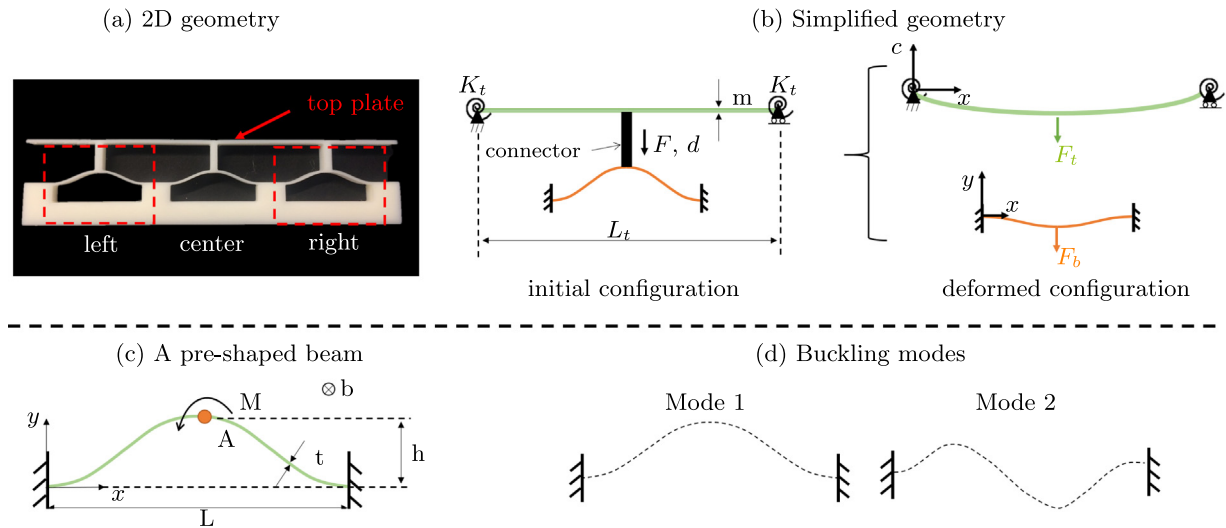
(a) 2D geometry

(b) Simplified geometry

(c) A pre-shaped beam

(d) Buckling modes

Fig. 4. Modeling the snap-through transition. (a) A physical demonstration of a basic structural element. (b) Illustration of the simplified geometry. The top plate is assumed as a straight beam (in green) and the center bi-stable element is simplified as a pre-shaped beam (in orange). Left and right bi-stable elements are simplified as two torsional springs with a rotational stiffness (K_t). (c) The stiffness K_t arises from rotation of a pre-shaped beam subjected to a moment at Point A ($x = L/2$). (e) Illustration of the first two buckling modes for a clamped–clamped straight beam under axial compression.

In order to realize a deterministic snapping sequence, small variations in the structural geometry can be introduced to different layers [41]. Measured force–displacement curves are displayed in Fig. 3(b), where two sequential snap-through responses are captured. Moreover, different L_t are taken and results in Fig. 3(c) show the κ decreases when increasing L_t. Considering the effect of h as discussed before, it can be expected that the curvature κ can be effectively tuned via controlling h/L_t. Note that the soft elastomer allows for large elastic deformations, enabling that the curved configurations can be fully reversed back to the initial state and be reusable. When using stiffer materials which typically allow smaller elastic strains, it is important to evaluate the maximum strain for avoiding plastic deformations and material failure and to adapt the design accordingly.

3.2. Bi-stability criterion

In the previous section, it is found that the snap-through response from the initial to the curved stable configuration can be tuned by varying the bi-stable elements' geometric parameters. Here, an analytical model is developed to study the relation between the geometric parameters and the structural stability.

3.2.1. Model description

As shown in Fig. 4(a), the structure is composed of three bi-stable elements (left, center, and right) and a top plate. Note that the transition from the initially flat to the curved stable configuration involves: (i) the snap-through of the center element; (ii) rotations of the left and right (adjacent) bi-stable elements; (iii) deformations of the top plate. Here, a simplified 2D structural geometry is proposed, as illustrated in Fig. 4(b). In this figure, the straight beam (marked in green) represents the top plate, and the center bi-stable element shown in Fig. 4(a) is simplified as a pre-shaped beam (highlighted in orange). To capture the rotational deformation of adjacent elements, we introduce two torsional springs with a rotational stiffness K_t on either end of the straight beam (see Fig. 4(b)). In doing so, the left and right bi-stable elements in Fig. 4(a) are simplified as two torsional springs in the model. Therefore, the geometry here consists of one straight beam, one pre-shaped beam at the center combined with a rigid connector (in black), and two torsional springs at two ends (see Fig. 4(b)) .

As shown in Fig. 4(b), a vertical displacement (d) is prescribed at the rigid connector and the resulting force F is calculated. Note that both the straight and the pre-shaped beam experience the same vertical displacement (d) at the center. Thus, F can be decomposed into two parts, namely:

$$F = F_t + F_b, \tag{3}$$

where F_t is the resulting force related to the straight beam's deformation and F_b represents the force associated with the curved center beam's deflection (see Fig. 4(b)). Here, we solve F by calculating F_t and F_b separately. Note that notations (t, h, L, m, b and L_t) shown in Fig. 4 are consistent with those defined before.

a. Calculation of K_t

For deriving F_t, it is necessary to first determine the rotational stiffness K_t. As discussed before, K_t results from the rotations of adjacent elements (i.e., pre-shaped beams). That is, when a moment (M) is applied at the center of a pre-shaped beam (see Fig. 4(c)), K_t can be obtained by calculating the slope of $M - \theta$ curve, where θ is the resulting rotation at Point A in the figure. Previous studies have shown that for a pre-shaped beam, employing buckling modes as bases can give a good approximation of the snap-through behavior [33,39]. Here, the $M - \theta$ relation is derived based on the principle of mode superposition and minimum total potential energy. According to Euler–Bernoulli theory [42], buckling modes of a clamped–clamped beam under axial compression can be expressed as:

$$y_i = 1 - \cos(N_i \frac{x}{L}) \quad \text{and} \quad N_i = (i+1)\pi, \quad \text{when} \quad i = 1, 3, 5... \tag{4}$$

$$y_i = 1 - 2\frac{x}{L} - \cos(N_i \frac{x}{L}) + \frac{2}{N_i} \sin(N_i \frac{x}{L}) \quad \text{and}$$
$$N_i = 2.86\pi, 4.92\pi, 6.94\pi ... \quad \text{when} \quad i = 2, 4, 6... \tag{5}$$

where y_i represents ith buckling mode in the x–y coordinate system shown in Fig. 4(c). The first two mode shapes are illustrated in Fig. 4(d). Using the buckling modes, the beam's deformed shape (y) under a moment can be defined as:

$$y = \sum_{i \in \{1,2,4,6,8\}} A_i y_i \quad \text{and} \quad y_0 = \frac{h}{2} y_1, \tag{6}$$

where y_0 represents the initial curved shape. As the beam's deformed shape will be asymmetric when a moment is applied at the center, asymmetric buckling modes (Mode 2, 4, 6, 8) are adopted in Eq. (6). A row vector is defined as $\mathbf{A} = \{A_1, A_2, A_4, A_6, A_8\}$, which includes the unknown coefficients that need to be solved. Next, governing equations can be obtained by taking the derivative of total potential energy with respect to each component in $\mathbf{A}$. We solve the resulting system of equations numerically by scanning M in a certain range, by which $\mathbf{A}$ and the $M - \theta$ curves can be obtained (see Supporting Material, Appendix A).

b. Derivation of F_t

With the derived K_t, we can calculate the straight beam's deformation and the associated force F_t. For a flat beam, when the force F_t is applied at the center (i.e., $x = L_t/2$), as presented in Fig. 4(b), the resulting displacement can be expressed as:

$$c(x) = \frac{S_1}{6}x^3 + \frac{S_2}{2}x^2 + S_3 x + S_4 \quad \text{for} \quad x \in [0, \frac{L_t}{2}], \tag{7}$$

where $c(x)$ is a Cartesian coordinate system depicted in Fig. 4(b), and S_1, S_2, S_3, S_4 are unknown coefficients. By substituting boundary conditions, relation between F_t and d is derived as:

$$d = c(\frac{L_t}{2}) = \frac{-F_t}{12EI_t}(\frac{L_t}{2})^3 + \frac{F_t L_t^2}{32EI_t(\frac{L_t}{2} + \frac{EI_t}{K_t})}(\frac{L_t}{2})^2$$

$$+ \frac{F_t L_t^2}{8K_t L_t + 16EI_t}(\frac{L_t}{2}), \tag{8}$$

where EI_t is the bending stiffness of the straight beam. The detailed derivation for Eq. (8) can be found in Supporting Material (see Appendix A).

c. Derivation of F_b

Next, the force F_b related to the beam's snap-through is calculated. For the pre-shaped beam subjected to a vertical force (F_b) in the center, as demonstrated in Fig. 4(b), the corresponding load–displacement response can be derived based on the mode superposition principle, similar to the procedure we discussed before for deriving the rotational stiffness. Here, the first nine symmetric buckling modes are employed as basis and the deformed shape is expressed as:

$$y = \sum_{i \in \{1,3,5,7,9\}} B_i y_i, \tag{9}$$

where $\mathbf{B} = \{B_1, B_3, B_5, B_7, B_9\}$ represents unknown coefficients and y_i is the buckling mode (see Eq. (4)). Here, it is assumed that the center beam will exhibit symmetric deformations under the prescribed displacement d, and thus the symmetric buckling modes are employed in the equation. The total potential energy consists of the strain energy (U_s) as a function of $\mathbf{B}$ and the potential energy (U_p) due to the load F_b, namely:

$$U = U_s(\mathbf{B}) + U_p \quad \text{and} \quad U_p = -F_b d. \tag{10}$$

Based on the minimum total potential energy principle, a system of five equations is obtained, which can be solved numerically (see Supporting Material, Appendix A).

3.2.2. Model results

Following the discussed procedure, we first look into K_t as predicted by the analytical model. In particular, Fig. 5(a) shows M-θ curves for beams with different geometric parameters, where K_t is the tangent slope of each curve. From the figure it can be noted that a good agreement between the analytical and numerical result is realized, verifying the proposed model. In addition, it can be seen that K_t is dependent on both h/L and t/L. Using the analytical model, the influence of h and t on K_t are studied,

as plotted in Fig. 5(b). Note that K_t in the figure is obtained by computing the tangent slope to the $M - \theta$ curve at rotation θ= 0.2. From the figure, it can be seen that K_t is sensitive to the variation of t/L, while varying h/L has a smaller effect on K_t as opposed to t/L. This is mainly due to the fact that varying t has a significant influence on the structural bending stiffness as well as the bending energy during deformations. Therefore, the rotational stiffness of a pre-shaped beam can be effectively tuned by changing the thickness t.

Snap-through transitions predicted by the analytical model are presented in Fig. 5(c). To validate the model, results from finite element simulations are added, as shown in the figure. It can be seen that the model is able to predict the snap-through response properly. Both analytical and numerical results confirm that the snap-through characteristics can be tuned by changing the geometric parameters (e.g., h/L and t/L). Moreover, the effect of m on F_{min} is also studied, as shown in Fig. 5(d). It can be noted that the model is able to capture the relation between m and F_{min} accurately such that increasing m could cause $F_{min} > 0$, eliminating the existence of the deformed stable configuration. Using the analytical model, it is possible to provide a quick estimate of the maximum value of m which still leads to a stable deformed configuration.

Using this analytical model, we study the bi-stability criterion that enables the top plate to maintain the curved configurations. As shown in Fig. 6(a) and (b), phase diagrams allowing for the stable curved configuration are defined on the basis of the normalized quantities (h/L and t/L). In particular, these figures display the variation of $|F_{min}|$ (absolute value) and F_{max} with respect to h/L and t/L. The colored region indicates configurations at which the top plate is able to stabilize ($F_{min} < 0$), while the gray area indicates that the plate recovers to the initial configuration after removing the loads (i.e. mono-stable behavior). It can be interpreted that when h/L of bi-stable elements is given, the corresponding t/L needs to be selected within a certain range in order to realize the stable curved configuration. When t/L is smaller than a certain value (0.012 as shown in Fig. 6(a)), mono-stable behavior occurs. In order to realize stable configurations, t/L and h/L need to be larger than 0.013 and 0.045, respectively, as highlighted in Fig. 6(a). In addition, the boundary that distinguishes the stable and mono-stable state is approximated as:

$$\frac{t}{L} = 0.41 * \frac{h}{L} - 0.00545, \tag{11}$$

as denoted in Fig. 6(a). It can be interpreted that for a given h/L, the maximum t/L allowing for the stable configuration can be calculated using Eq. (11). This is because a small t/L cannot provide sufficient F_{min} for the top plate to maintain the deformed state, while a very large t/L will make the center element diminish bi-stability. In addition, it can be observed that F_{max} and $|F_{min}|$ exhibit different sensitivities for parameter variations. To maximize F_{max}, large h/L and t/L are required. In case of $|F_{min}|$, it shows a nonlinear relation with respect to t/L. That is, further increasing t/L will lead to a decrease of $|F_{min}|$, resulting in mono-stable behavior. Using the proposed model, we can rapidly identify the region for realizing curved stable configurations and select proper geometric parameters.

4. 2D arrangements of bi-stable units

As discussed in Section 2.1, for the top plate, 2D arrangements of bi-stable units can lead to multiple curved configurations oriented in different directions. This section presents the multi-stable metastructures with 2D arrangements of bi-stable elements and studies the deformed configurations for the top
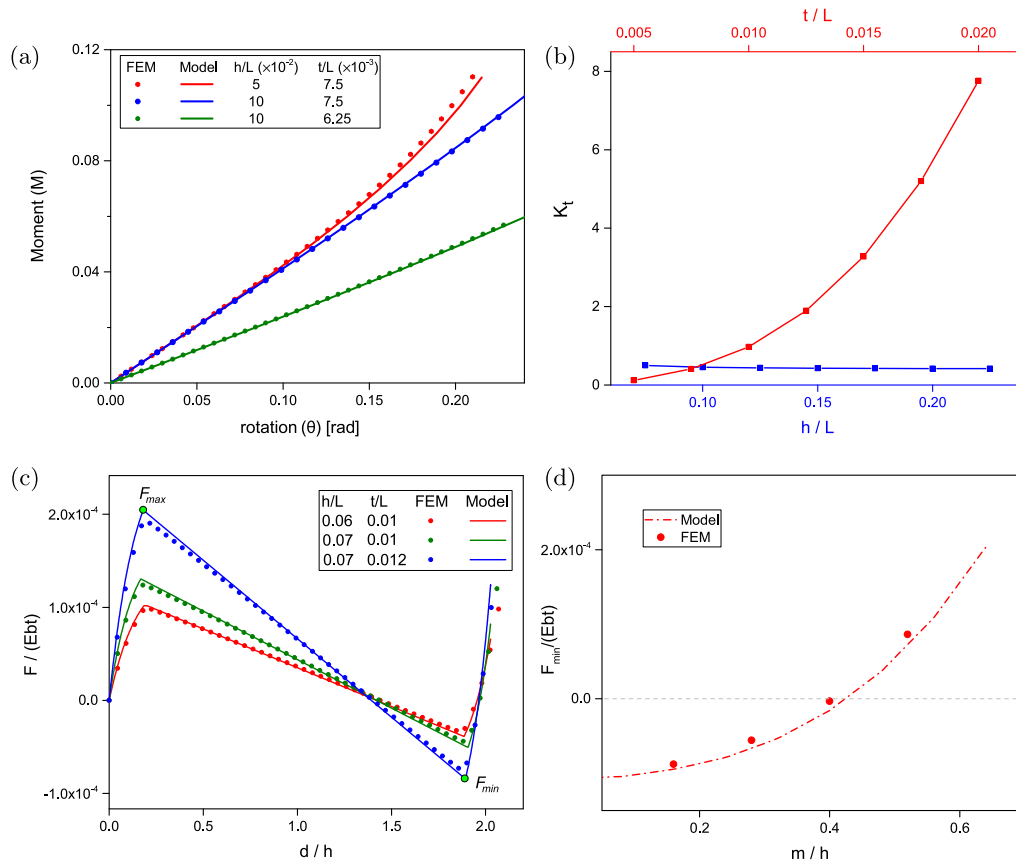
Fig. 5. The predicted K_t and force–displacement responses from the analytical model. (a) The moment versus rotation ($M - \theta$) for a pre-shaped beam (b = 4 mm) when subjected to an applied moment. The torsional stiffness K_t can be derived by calculating the tangent slope of $M(\theta)$, as denoted in this figure. (b) Effects of h/L and t/L on K_t are investigated analytically. Here, t/L is taken as 7.5×10^{-3} when varying h/L, while in case of changing t/L, h/L is kept unchanged as 6.25×10^{-2}. (c) A comparison of snap-through responses predicted by the analytical model and FEM. (d) Effect of m on the structural stability, i.e., F_{min}.
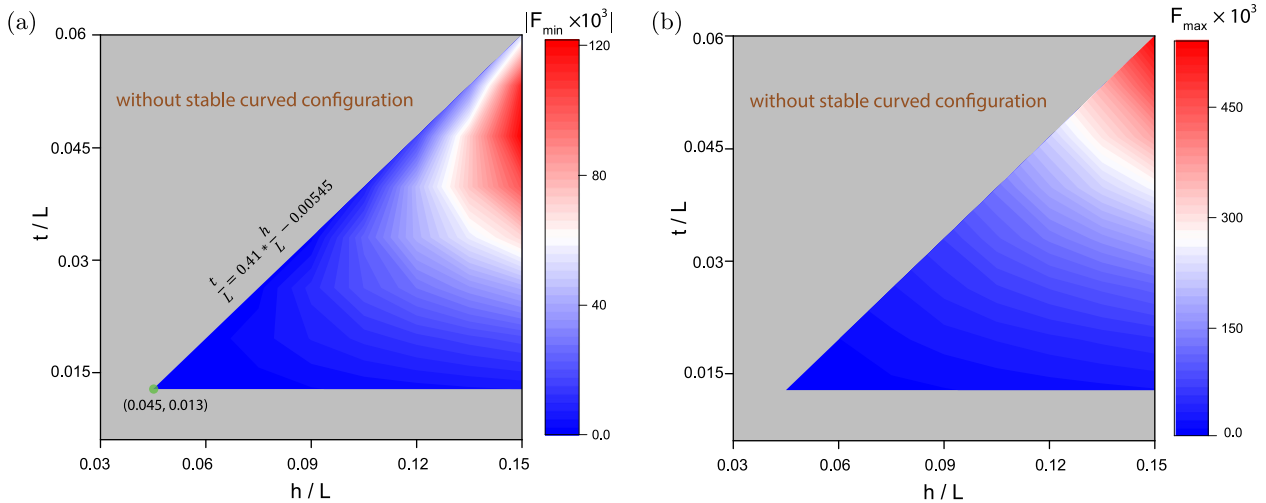

Fig. 6. Stability criterion for the curved stable configuration. (a)–(b) The variation of F_{max} and $|F_{min}|$ as a function of t/L and h/L. The proper design space for realizing the stable curved configuration is denoted in color, while the gray region represents mono-stable behavior. The latter indicates the structure cannot retain the stable curved configuration.

plate. Here, multi-stable metastructures are designed by considering an in-plane periodic arrangement of bi-stable units. The unit based on the snapping beam is illustrated in Fig. 7(a), where the picture on the right shows an experimental demonstration of a multi-stable metastructure consisting of 4 × 4 bi-stable units. A thin plate is then connected with the multi-stable metastructure at the top.

Through controlling snap-through deformations locally, the structure is capable of achieving a series of deformed stable configurations. Fig. 7(b) displays a few stable configurations of the top plate, where the dashed red lines highlight bi-stable units that have snapped into the second stable state. From the figure, it can be noted that the top plate can not only exhibit curved stable states in x and y direction, but also is able to realize
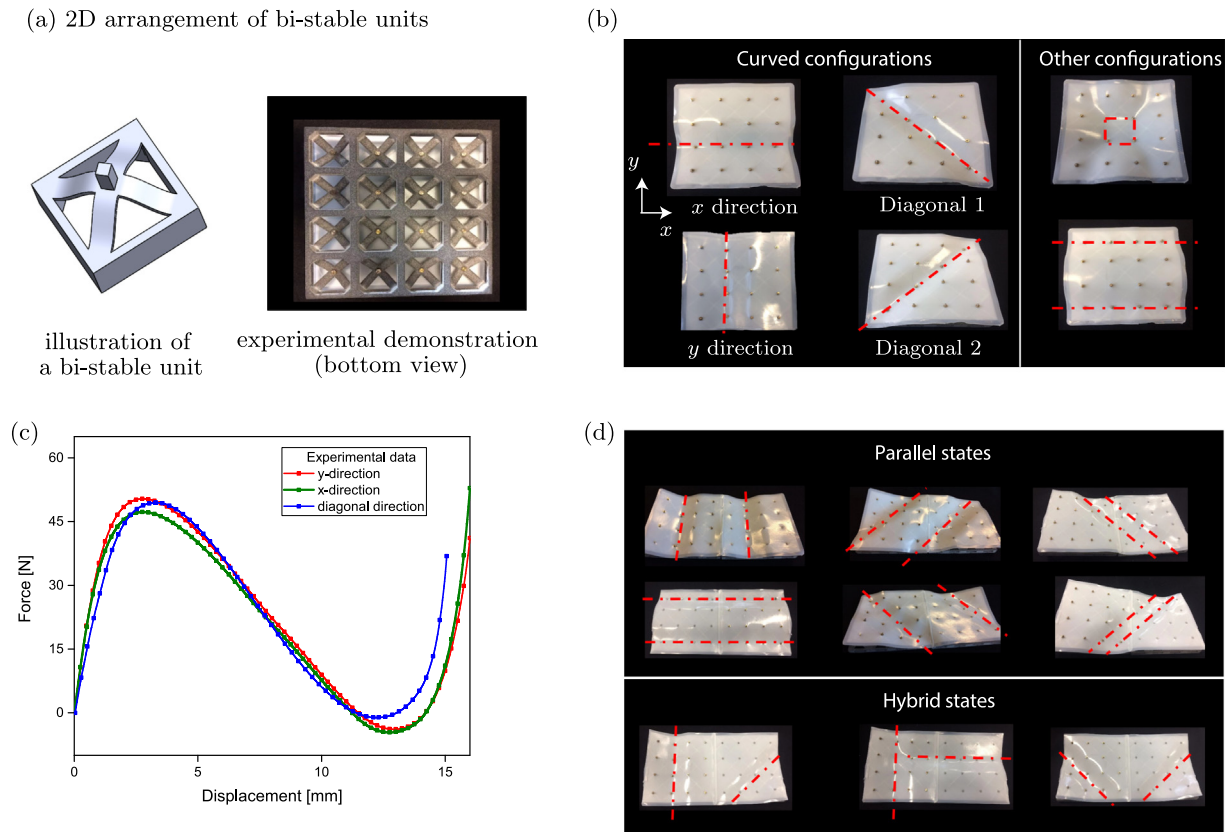
Fig. 7. Multi-stable surface designs based on 2D arrangements of bi-stable units. (a) A bi-stable unit based on the snapping beam is illustrated. On the right, an experimental demonstration of the metastructure is displayed. (b) The representative deformed stable configurations of the top plate. (c) Measured force–displacement curves corresponding to transitions from the initial to x direction, y direction, and Diagonal 1 configuration. (d) By combining more bi-stable elements, multiple stable deformed configurations, including the parallel and hybrid states, can be realized.

stable deformations in two diagonal orientations (denoted as Diagonal 1 and 2 in Fig. 7(b)). The multiple curved configurations in different directions are mainly caused by the in-plane arrangement of bi-stable elements as well as the compliance of the plate. Here, we characterize the snap-through transitions from the initial to x direction, y direction, and Diagonal 1 configuration, respectively. For each configuration, a displacement-controlled loading is applied to the units highlighted by the dashed red lines and the total force is measured. Results in Fig. 7(c) indicate that the three snap-through transitions exhibit similar force–displacement characteristics. This is due to the fact that the snap-through response of each case mainly results from deformations of the top plate and four snapped bi-stable units. Thus, critical loads are almost the same for all three cases. Moreover, it should be noted that other stable configurations can also be realized. For instance, deforming four bi-stable elements in the middle can result in a local curvature for the plate, as shown in Fig. 7(b).

By arranging more bi-stable units, more stable configurations can be realized. Here, we build a multi-stable metastructure with an arrangement of 8 × 4 bi-stable elements and connect it with a thin plate. As demonstrated in Fig. 7(d), various morphological states can be achieved. The deformed configurations can be classified into two representative groups: parallel and hybrid states. That is, two parallel curved configurations can be achieved in x, y, and diagonal directions, respectively (see Fig. 7(d)). The hybrid stable states in the figure demonstrate that it is possible to combine two curved configurations with different directions to generate hybrid deformed states, making surface morphology distinct from the parallel states.

However, it should be noted that arranging a large number of bi-stable units may limit further extension of the parallel and hybrid states. This is because when more units are arranged, the surface's in-plane motions will be constrained, generating large resistant forces against the stable deformed configurations. In order to address this, surfaces consisting of meso-structures can be employed for mitigating effects of the in-plane deformations. Previous studies have demonstrated that introducing mesostructures into a plate can be an effective way to design highly flexible surfaces with low in-plane stiffness [43,44]. In doing so, it is possible to extend the presented stable configurations (e.g., parallel and hybrid states) to a large extent. Here, we design a mesostructure-based surface comprising curved leaf springs, as shown in Fig. 8(a). Specifically, a multi-stable metastructure consisting of 16 × 8 bi-stable elements and a meso-surface are manufactured through 3D printing, respectively. The planar structure is then connected to a multi-stable metastructure. By controlling multiple units' snap-through deformations, a series of surface morphology can be obtained. Specifically, parallel states in y direction are presented in Fig. 8(b), which verifies the feasibility of extending the stable states to a large extent. Moreover, Fig. 8(c) shows that the curved stable configurations can be effectively aligned in different directions, as denoted by the red dashed lines. To highlight this, a rubber sheet (the red surface in Fig. 8(c)) is placed on top of the planar structure, which clearly shows the deformed configurations that mimic corrugated patterns. It can be expected that based on the proposed design, the stable patterns can be further extended by adding more bi-stable elements. Note that each bi-stable element is capable of deforming independently, enabling a number of stable patterns. Fig. 8(d) presents one of the irregular stable configurations of
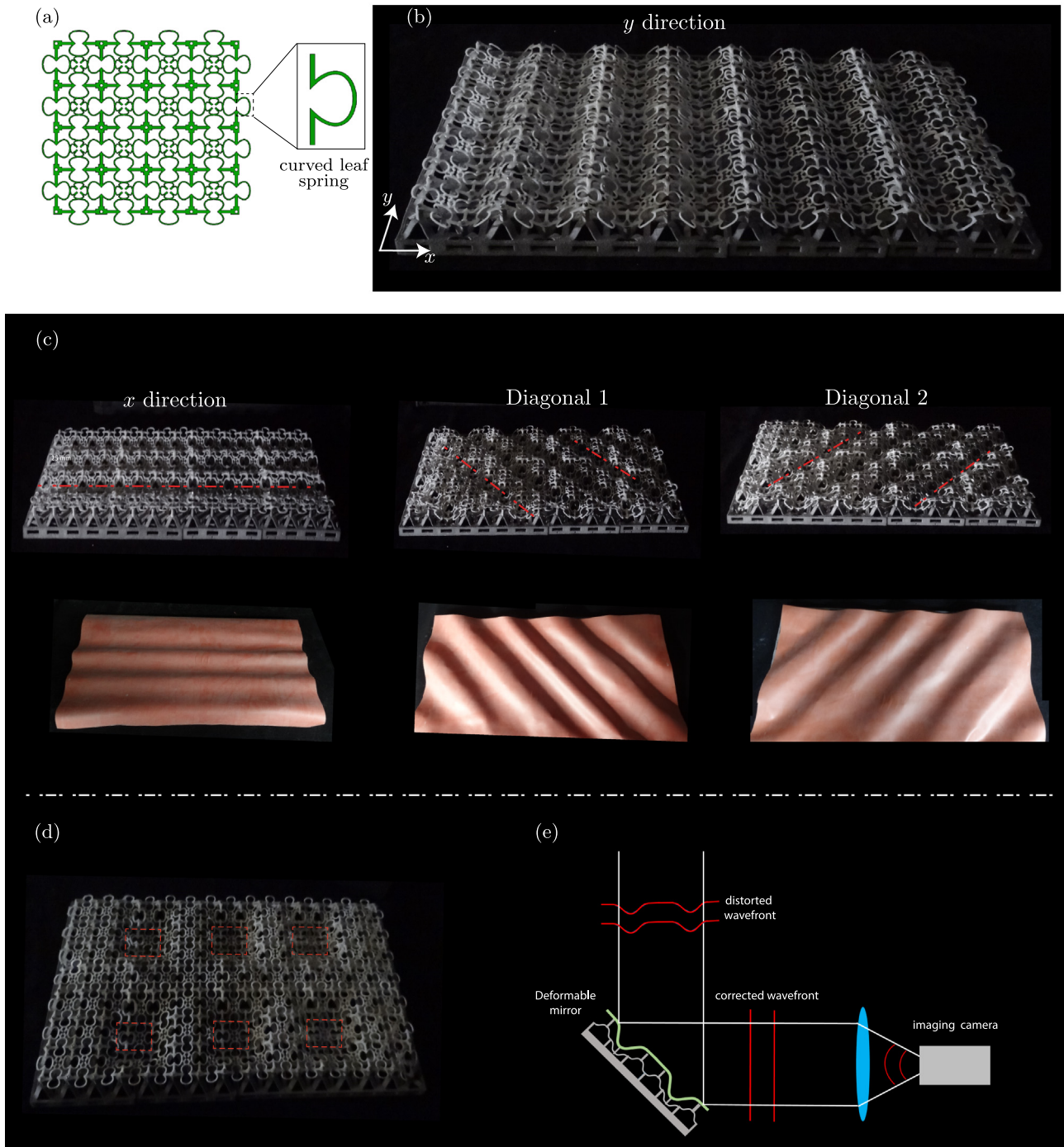
Fig. 8. Programming of curved stable configurations via arranging a large number of bi-stable units. (a) A mesostructure-surface design is based on curved leaf springs. The illustrated curved leaf spring on the right can exhibit relatively large in-plane compliance. (b) Photograph of the manufactured structure demonstrates multiple parallel stable configurations enabled by a multi-stable metastructure (16 × 8 units) and the mesostructure-based surface design. (c) The parallel states can be oriented in different directions to realize corrugated patterns, as highlighted by the red dashed lines. (d) One irregular stable pattern of the multi-stable surface. (e) The potential application of the multi-stable surfaces as deformable mirrors.

the surface and other demonstrations can be found in Supporting Materials. The multiplicity of surface morphology can be useful for some applications, such as morphing airfoils and adaptive optics. Here, an illustrative example for the adaptive optics is shown in Fig. 8(e), where a deformable mirror is normally needed to generate high-resolution images. As presented in the figure, the designed structure could act as a compliant mirror with tunable surface shapes such that the distorted wavefront can be

corrected by changing the surface patterns. In doing so, high-resolution images can be captured by the camera. Importantly, the deformed shapes can be retained stable, avoiding prolonged actuation.

5. Conclusions

This work presents a design of multi-stable surfaces based on beam-type metastructures. The presented design allows for

a series of curved configurations in multiple directions, enabled by a collective effect of the beams' bi-stability and the surface's compliance. The snap-through deformations of the structures are investigated, and effects of geometric parameters are analyzed. Results show that h/L of the bi-stable element is important for tuning the stable curvature, while t/L plays a paramount role in adjusting the snap-through response. Moreover, an analytical model that can accurately predict the snap-through transition is proposed. Using the model, the design criterion for realizing stable configurations is studied as a function of h/L and t/L. It is found that in order to achieve a stable configuration, h/L should be large, while t/L needs to be constrained within a certain range. This criterion can serve as a guideline for tuning the snap-through response and manipulating stability of the deformed states. Moreover, we have applied this design concept to 2D arrangements of bi-stable units and have demonstrated the resulting stable configurations (e.g., parallel and hybrid states). In order to extend the deformed configurations to a large extent, a meso-structure based surface is designed. It is demonstrated that the stable configurations can be extended further with the meso-structure based surfaces, enabling corrugations in different directions. With proper arrangements of bi-stable elements, the proposed design can be explored to develop functional surfaces with tunable properties.

Declaration of competing interest

The authors declare that they have no known competing financial interests or personal relationships that could have appeared to influence the work reported in this paper.

Acknowledgments

Appendix A. Supplementary data

Supplementary material related to this article can be found online at https://doi.org/10.1016/j.eml.2021.101553.

References

[1] S. Barbarino, O. Bilgen, R.M. Ajaj, M.I. Friswell, D.J. Inman, A review of morphing aircraft, J. Intell. Mater. Syst. Struct. 22 (9) (2011) 823–877.

[2] C.G. Diaconu, P.M. Weaver, F. Mattioni, Concepts for morphing airfoil sections using bi-stable laminated composite structures, Thin-Walled Struct. 46 (6) (2008) 689–701.

[3] G. Arena, R. MJ Groh, A. Brinkmeyer, R. Theunissen, P. M. Weaver, A. Pirrera, Adaptive compliant structures for flow regulation, Proc. R. Soc. A: Math. Phys. Eng. Sci. 473 (2204) (2017) 20170334.

[4] S. Daynes, P. Weaver, J. Trevarthen, A morphing composite air inlet with multiple stable shapes, J. Intell. Mater. Syst. Struct. 22 (9) (2011) 961–973.

[5] J. Wu, J. Li, S. Yan, Design of deployable bistable structures for morphing skin and its structural optimization, Eng. Optim. 46 (6) (2014) 745–762.

[6] X. Lachenal, S. Daynes, P.M. Weaver, Review of morphing concepts and materials for wind turbine blade applications, Wind Energy 16 (2) (2013) 283–307.

[7] Y. Lu, H. Yue, Z. Deng, H. Tzou, Distributed sensing signal analysis of deformable plate/membrane mirrors, Mech. Syst. Signal Process. 96 (2017) 393–424.

[8] M. Hendrikx, J. ter Schiphorst, E.P. van Heeswijk, G. Koçer, C. Knie, D. Bléger, S. Hecht, P. Jonkheijm, D.J. Broer, A.P. Schenning, Re-and preconfigurable multistable visible light responsive surface topographies, Small 14 (50) (2018) 1803274.

[9] Y. Shen, Q. Zou, B. Wan, X. She, R. You, Y. Luo, C. Jin, High-contrast dynamic reflecting system based on pneumatic micro/nanoscale surface morphing, ACS Appl. Mater. Interfaces (2020).

[10] O. Peretz, A.K. Mishra, R.F. Shepherd, A.D. Gat, Underactuated fluidic control of a continuous multistable membrane, Proc. Natl. Acad. Sci. 117 (10) (2020) 5217–5221.

[11] S. Jiao, M. Liu, Snap-through in graphene nanochannels: With application to fluidic control, ACS Appl. Mater. Interfaces (2020).

[12] Y. Park, G. Vella, K.J. Loh, Bio-inspired active skins for surface morphing, Sci. Rep. 9 (1) (2019) 1–10.

[13] Y. Park, K.J. Loh, Surface morphing of geometrically patterned active skins, MRS Adv. 5 (14) (2020) 743–750.

[14] D.P. Holmes, A.J. Crosby, Snapping surfaces, Adv. Mater. 19 (21) (2007) 3589–3593.

[15] N. Hu, R. Burgueño, Buckling-induced smart applications: recent advances and trends, Smart Mater. Struct. 24 (6) (2015) 063001.

[16] D.P. Holmes, Elasticity and stability of shape-shifting structures, Curr. Opin. Colloid Interface Sci. 40 (2019) 118–137.

[17] S. Guest, S. Pellegrino, Analytical models for bistable cylindrical shells, Proc. R. Soc. A: Math. Phys. Eng. Sci. 462 (2067) (2006) 839–854.

[18] A.F. Arrieta, I.K. Kuder, T. Waeber, P. Ermanni, Variable stiffness characteristics of embeddable multi-stable composites, Compos. Sci. Technol. 97 (2014) 12–18.

[19] A. Madhukar, D. Perlitz, M. Grigola, D. Gai, K.J. Hsia, Bistable characteristics of thick-walled axisymmetric domes, Int. J. Solids Struct. 51 (14) (2014) 2590–2597.

[20] Z. Chen, Q. Guo, C. Majidi, W. Chen, D.J. Srolovitz, M.P. Haataja, Nonlinear geometric effects in mechanical bistable morphing structures, Phys. Rev. Lett. 109 (11) (2012) 114302.

[21] M. Alturki, R. Burgueño, Response characterization of multistable shallow domes with cosine-curved profile, Thin-Walled Struct. 140 (2019) 74–84.

[22] A. Brinkmeyer, M. Santer, A. Pirrera, P. Weaver, Pseudo-bistable self-actuated domes for morphing applications, Int. J. Solids Struct. 49 (9) (2012) 1077–1087.

[23] M. Taffetani, X. Jiang, D.P. Holmes, D. Vella, Static bistability of spherical caps, Proc. R. Soc. A: Math. Phys. Eng. Sci. 474 (2213) (2018) 20170910.

[24] E. Loukaides, K. Seffen, Multistable grid and honeycomb shells, Int. J. Solids Struct. 59 (2015) 46–57.

[25] Y. Cui, M. Santer, Highly multistable composite surfaces, Compos. Struct. 124 (2015) 44–54.

[26] F. Dai, H. Li, S. Du, A multi-stable wavy skin based on bi-stable laminates, Composites A 45 (2013) 102–108.

[27] F. Dai, H. Li, S. Du, Design and analysis of a tri-stable structure based on bi-stable laminates, Composites A 43 (9) (2012) 1497–1504.

[28] Y. Cui, M. Santer, Characterisation of tessellated bistable composite laminates, Compos. Struct. 137 (2016) 93–104.

[29] A. Norman, K. Seffen, S. Guest, Multistable corrugated shells, Proc. R. Soc. A: Math. Phys. Eng. Sci. 464 (2095) (2008) 1653–1672.

[30] G. Risso, M. Sakovsky, P. Ermanni, Highly multi-stable FRP grids for shape adaptation, in: AIAA Scitech 2021 Forum, 2021, p. 1493.

[31] S. Shan, S.H. Kang, J.R. Raney, P. Wang, L. Fang, F. Candido, J.A. Lewis, K. Bertoldi, Multistable architected materials for trapping elastic strain energy, Adv. Mater. 27 (29) (2015) 4296–4301.

[32] Y. Zhang, Q. Wang, M. Tichem, F. van Keulen, Design and characterization of multi-stable mechanical metastructures with level and tilted stable configurations, Extreme Mech. Lett. 34 (2020) 100593.

[33] K. Che, C. Yuan, J. Wu, H. Jerry Qi, J. Meaud, Three-dimensional-printed multistable mechanical metamaterials with a deterministic deformation sequence, J. Appl. Mech. 84 (1) (2017).

[34] S.M. Montgomery, X. Kuang, C.D. Armstrong, H.J. Qi, Recent advances in additive manufacturing of active mechanical metamaterials, Curr. Opin. Solid State Mater. Sci. 24 (5) (2020) 100869.

[35] T. Frenzel, C. Findeisen, M. Kadic, P. Gumbsch, M. Wegener, Tailored buckling microlattices as reusable light-weight shock absorbers, Adv. Mater. 28 (28) (2016) 5865–5870.

[36] D. Restrepo, N.D. Mankame, P.D. Zavattieri, Phase transforming cellular materials, Extreme Mech. Lett. 4 (2015) 52–60.

[37] F. Bobbert, S. Janbaz, T. van Manen, Y. Li, A. Zadpoor, Russian doll deployable meta-implants: Fusion of kirigami, origami, and multi-stability, Mater. Des. 191 (2020) 108624.

[38] X. Liu, F. Lamarque, E. Doré, P. Pouille, Multistable wireless micro-actuator based on antagonistic pre-shaped double beams, Smart Mater. Struct. 24 (7) (2015) 075028.

[39] J. Qiu, J.H. Lang, A.H. Slocum, A curved-beam bistable mechanism, J. Microelectromech. Syst. 13 (2) (2004) 137–146.

[40] R. Marlow, A general first-invariant hyperelastic constitutive model, Const. Models Rubber (2003) 157–160.

[41] K. Che, C. Yuan, J. Wu, H.J. Qi, J. Meaud, Three-dimensional-printed multistable mechanical metamaterials with a deterministic deformation sequence, J. Appl. Mech. 84 (1) (2017) 011004.

[42] S.P. Timoshenko, J.M. Gere, Theory of Elastic Stability, Courier Corporation, 2009.

[43] T. van Manen, S. Janbaz, M. Ganjian, A.A. Zadpoor, Kirigami-enabled self-folding origami, Mater. Today 32 (2020) 59–67.

[44] M.J. Mirzaali, A. Ghorbani, K. Nakatani, M. Nouri-Goushki, N. Tümer, S.J.P. Callens, S. Janbaz, A. Accardo, J. Bico, M. Habibi, A.A. Zadpoor, Curvature induced by deflection in thick meta-plates, Adv. Mater. (2021) 2008082.